DOI: 10.1002/anie.201003080

Perovskites

$(In_{1-y}Mn_y)MnO_3$ ($1/9 \le y \le 1/3$): Unusual Perovskites with Unusual Properties**

Alexei A. Belik, Yoshitaka Matsushita, Masahiko Tanaka, and Eiji Takayama-Muromachi*

The perovskite-type ABO_3 structure is highly adaptive. There are hundreds of perovskite-type compounds.[1] Many of them have extremely important technological properties, for example $BaTiO_3$, $SrTiO_3$, $SrRuO_3$, and $Pb(Zr_{1-x}Ti_x)O_3$. Applications of perovskites range from use as catalysts or sensors to superconductors and ferromagnetic or ferroelectric materials.[1] Among perovskites, (doped) manganites $LnMnO_3$ (Ln = La–Lu) have been investigated a lot in the last decades because of the colossal magnetoresistance and orbital/charge ordering phenomena.[2,3] The discovery of multiferroic properties of $LnMnO_3$ (Ln = Tb–Lu) has attracted new interest to these systems.[4,5]

$LnMnO_3$ (Ln = La–Lu) compounds are divided into two groups: perovskites $LnMnO_3$ (Ln = La–Dy) and hexagonal $LnMnO_3$ (Ln = Y, Ho–Lu). The perovskite modification can be stabilized for all members of $LnMnO_3$ (Ln = La–Lu) using a high-pressure synthesis or other methods. The magnetic phase diagram for perovskites $LnMnO_3$ (Ln = La–Lu) is well established, and there are two magnetic phases with long-range ordering and multiferroic properties for small Ln^{3+} ions.[3–5] With decreasing radius of Ln^{3+} ions, the Jahn–Teller distortion increases and the competition between nearest-neighbor and next-nearest-neighbor interactions is enhanced.[3] Are there any possibilities to extend the existing phase diagram of $LnMnO_3$? The hexagonal modification is known for smaller ions, such as in $ScMnO_3$, and $InMnO_3$.[6,7] However, $ScMnO_3$ and $InMnO_3$ perovskites have never been reported, even though attempts to stabilize new phases of $ScMnO_3$ and $InMnO_3$ have been made.[8] Note that $ScCrO_3$,[9] $InCrO_3$, and $InRhO_3$ perovskites can be prepared at high pressure.[10] Indium-based perovskites have recently attracted attention as new room-temperature multiferroic materials.[11–13]

Herein, we report on the stabilization of new perovskite oxides $(In_{1-y}Mn_y)MnO_3$ ($1/9 \le y \le 1/3$) using a high-pressure high-temperature technique. Not only is the discovery of new simple ABO_3 perovskites extremely rare these days, but $(In_{1-y}Mn_y)MnO_3$ perovskites are very unusual in a few ways. First, there is a significant number of Mn atoms at the A site of the perovskite structure together with Mn atoms at the B site, and the doping at the A site occurs by Mn^{2+} ions. Second, $(In_{1-y}Mn_y)MnO_3$ crystallizes in the B-site-ordered structure owing to ordering of Mn^{3+} and Mn^{4+} ions. Third, $(In_{1-y}Mn_y)MnO_3$ with $1/9 \le y \le 0.25$ demonstrates spin-glass-like magnetic properties in contrast to $LnMnO_3$ (Ln = La–Lu) but in agreement with $Ln_{1-y}Ca_yMnO_3$ (Ln = Y and Lu).

All the observed reflections on the synchrotron XRD pattern of $In_{0.6}MnO_{2.4}$ ($(In_{0.75}Mn_{0.25})MnO_3$) could be indexed in a monoclinic system with $a \approx 5.11$, $b \approx 5.31$, $c \approx 7.84$ Å, and $\beta \approx 92.19°$. Reflection conditions derived from the indexed reflections were $h+l=2n$ for $h0l$, $h00$, and $00l$ and $k=2n$ for $0k0$, affording one possible space group $P2_1/n$ (No. 14, cell choice 2). The lattice parameters and space group correspond to the monoclinically distorted $GdFeO_3$-type perovskite structure. Significant anisotropic broadening of reflections was observed in high-resolution synchrotron XRD data.[14] In general, reflections hkl and $-hkl$ had full width at half maximum values that differed by a factor of about two. Those reflections are the same in the absence of the monoclinic distortion ($\beta = 90°$). Anisotropic broadening is probably the effect of the high-pressure synthesis, and anisotropic broadening parameters were refined.

First, we started from the vacancy model $In_{1-x}MnO_{3-1.5x}$ ($x=0.4$), in which $g(\mathrm{In})=0.6$, $g(\mathrm{Mn1})=g(\mathrm{Mn2})=1$, and $g(\mathrm{O1})=g(\mathrm{O2})=g(\mathrm{O3})=0.8$, where g is the occupation factor. However, the fitting of some reflections was extremely poor.[14] The subsequent refinement of occupation factors resulted in $g(\mathrm{In})=0.88(1)$, $g(\mathrm{O1})=1.03(1)$, $g(\mathrm{O2})=1.00(1)$, and $g(\mathrm{O3})=1.07(1)$. This result showed that all the sites in $In_{1-x}MnO_{3-1.5x}$ ($x=0.4$) should be fully occupied, and the crystallographic formula will be $(In_{1-y}Mn_y)MnO_3$ ($y=0.25$; $y=x/(2-x)$) with $Z=4$ (where Z is the number of formula units per unit cell). The A site of the perovskite structure is occupied by In and Mn atoms. Table 1 gives crystallographic information resulting from the Rietveld refinement. Bond lengths, bond-valence sums (BVS),[15] distortion parameters of MnO_6 (Δ), a fragment of the crystal structure of $(In_{0.75}Mn_{0.25})MnO_3$, and observed, calculated, and difference

[*] Dr. A. A. Belik, Prof. E. Takayama-Muromachi
International Center for Materials Nanoarchitectonics (MANA)
National Institute for Materials Science (NIMS)
1-1 Namiki, Tsukuba, Ibaraki 305-0044 (Japan)
Fax: (+81) 29-860-4674
E-mail: alexei.belik@nims.go.jp
Homepage: http://www.nims.go.jp/mana/members/independent_scientist/a_Belik/index.html
Dr. Y. Matsushita, Dr. M. Tanaka
SPring-8 Office, NIMS
Kohto 1-1-1, Sayo-cho, Hyogo 679-5148 (Japan)

[**] This work was supported by World Premier International Research Center (WPI) Initiative on Materials Nanoarchitectonics (MEXT (Japan)), by the NIMS Individual-Type Competitive Research Grant, and by the Japan Society for the Promotion of Science (JSPS) through its "Funding Program for World-Leading Innovative R&D on Science and Technology (FIRST Program)". The synchrotron radiation experiments were performed at the SPring-8 with the approval of the Japan Synchrotron Radiation Research Institute (Proposal Numbers: 2009A4800 and 2009B4505).

Supporting information for this article is available on the WWW under http://dx.doi.org/10.1002/anie.201003080.

Table 1: Structural parameters of $(In_{0.75}Mn_{0.25})MnO_3$ at room temperature.[a]

Site	g	x	y	z	B [Å^2]
Mn1	1	0.5	0	0.5	0.14(3)
Mn2	1	0.5	0	0	0.73(3)
In	0.75	0.97960(10)	0.05806(6)	0.26387(8)	0.444(9)
Mn3	0.25	0.97960(10)	0.05806(6)	0.26387(8)	0.444(9)
O1	1	0.3661(5)	0.9369(6)	0.2733(3)	0.85(6)
O2	1	0.1786(7)	0.1967(6)	0.5489(4)	1.31(8)
O3	1	0.7049(7)	0.3081(6)	0.4144(4)	1.20(8)

[a] Space group $P2_1/n$ (no. 14, cell choice 2); $Z=4$; $a=5.11082(4)$, $b=5.30592(4)$, $c=7.83534(6)$ Å, $\beta=92.1896(4)°$, $V=212.320(3)$ Å^3, $R_{wp}=3.78\%$, $R_p=2.61\%$, $R_B=2.05\%$, and $R_F=0.91\%$. g is the occupation factor. The values of x, y, z, and B for the In and Mn3 sites were constrained to be the same. B is the isotropic thermal parameter.

synchrotron XRD patterns are given in the Supporting Information.

Figure 1 depicts XRD patterns of the $In_{1-x}MnO_{3-1.5x}$ samples with $x=0.1$, 0.2, 0.3, 0.4, and 0.5. $In_{0.9}MnO_{2.85}$ crystallizes in a hexagonal structure similar to stoichiometric $InMnO_3$.[7] The samples with $x=0.2$–0.5 had the perovskite-type structure. Weak reflections from unidentified impurities were detected in $In_{0.5}MnO_{2.25}$, indicating that this composition is the limit of stability of the perovskite structure. All the lattice parameters and the monoclinic angle decrease monotonically with increasing x.[14] The normalized volume (V/Z) drops by about 5.4% in the perovskite structure ($x=0.2$) compared with the hexagonal structure ($x=0.1$). In the stability range of the perovskite structure, the volume changes by about 0.9–1.0% with $\Delta x=0.1$.[14]

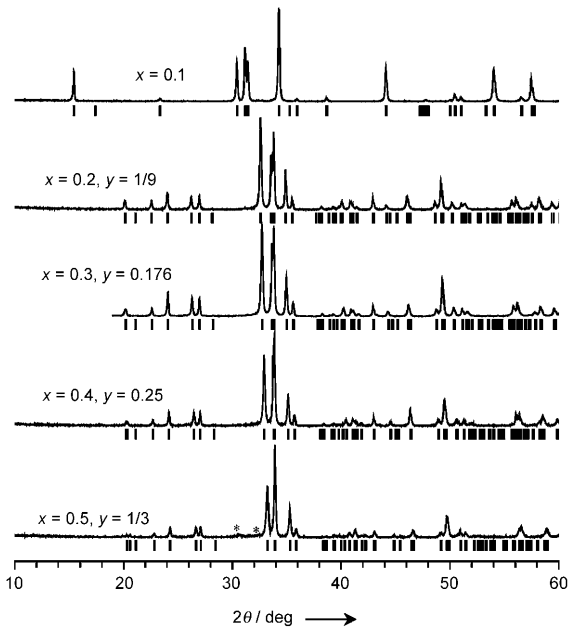

Figure 1. X-ray powder diffraction patterns of $In_{1-x}MnO_{3-1.5x}$ with $x=0.1$ (space group $P6_3cm$) and 0.2, 0.3, 0.4, and 0.5 (space group $P2_1/n$) measured with $Cu_{K\alpha}$ radiation at room temperature. Tick marks show the positions of possible Bragg reflections for the corresponding space groups. For perovskites, the formula can be rewritten as $(In_{1-y}Mn_y)MnO_3$ ($y=x/(2-x)$). Asterisks show reflections from unidentified impurities in $(In_{2/3}Mn_{1/3})MnO_3$.

Figure 2 shows the magnetic susceptibility (χ versus T) curves of $In_{1-x}MnO_{3-1.5x}$ ($x=0.2$, 0.3, 0.4, and 0.5). The curves for materials with $x=0.2$, 0.3, and 0.4 are typical for spin-glass-like materials. There are broad maxima on the zero-field-cooled (ZFC) curves and divergence between the ZFC

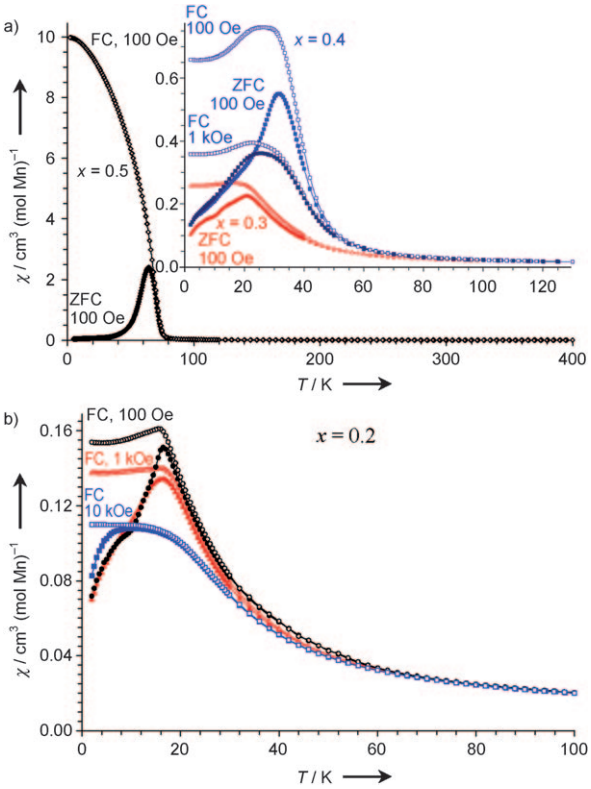

Figure 2. Temperature dependence of the ZFC (filled symbols) and FC (open symbols) direct-current magnetic susceptibility ($\chi=M/H$) curves of $In_{1-x}MnO_{3-1.5x}$. a) $x=0.5$ at 100 Oe. The inset shows the curves for $x=0.3$ at 100 Oe and for $x=0.4$ at 100 and 1000 Oe. b) $x=0.2$ at 0.1, 1, and 10 kOe.

and FC curves. The temperature position of the divergence shifts to lower temperatures with increasing magnetic field. The FC curves also show broad maxima and plateau-like behaviors at low temperatures. The χ versus T curves of $In_{0.5}MnO_{2.25}$ are typical for canted antiferromagnets, and such curves are usually observed in $GdFeO_3$-type materials (for example, in $LaMnO_3$). Figure 3 gives the inverse FC magnetic susceptibilities measured at 10 kOe. The experimental effective magnetic moments per mole of manganese ions and Curie–Weiss temperatures were almost the same in all the samples. However, the deviation from the linear Curie–Weiss behavior starts at higher temperatures with larger x. The calculated effective magnetic moments are almost the same, changing from 4.92 μ_B for $x=0.2$ to 4.95 μ_B for $x=0.5$. Plots of magnetic moment versus magnetic field strength (M vs. H) for $In_{1-x}MnO_{3-1.5x}$ ($x=0.2$, 0.3, 0.4) are also typical for spin-glass-like materials, with smeared hysteresis.[14] However, the well-defined hysteresis loop observed in $In_{0.5}MnO_{2.25}$ is typical for canted antiferromagnets (e.g. $LaMnO_3$).

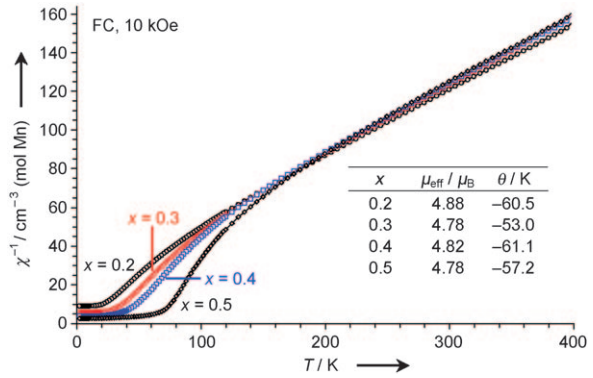

Figure 3. Temperature dependence of the inverse magnetic susceptibilities of $In_{1-x}MnO_{3-1.5x}$ ($x = 0.2$–0.5) measured at 10 kOe in the FC mode on cooling. The fitting results with the simple Curie–Weiss equation $\chi = \mu_{eff}^2/[8(T-\theta)]$ between 250 and 390 K are given.

Specific heat data are shown in Figure 4. Clear anomalies were found in $In_{1-x}MnO_{3-1.5x}$ ($x = 0.2$ and 0.5). However, the anomalies were rather rounded. On the other hand, almost no anomalies were observed in $In_{1-x}MnO_{3-1.5x}$ ($x = 0.3$ and 0.4). A magnetic field of 70 kOe smeared the anomalies and moved the magnetic part of specific heat to a high-temperature region, which is typical for spin glasses and ferromagnets.

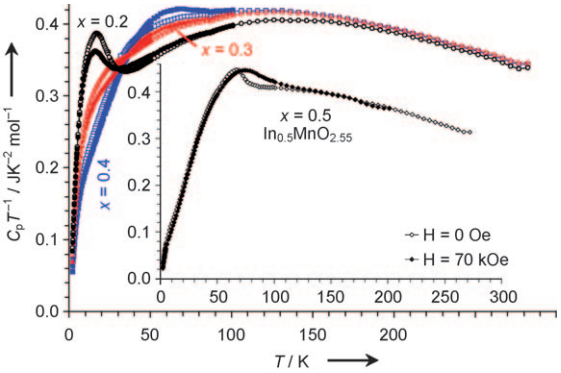

Figure 4. Temperature dependence of the specific heat of $In_{1-x}MnO_{3-1.5x}$ ($x = 0.2$–0.5) at 0 Oe (open symbols) and 70 kOe (filled symbols) plotted as C_p/T vs. T. The molecular weight here is calculated for $(In_{1-y}Mn_y)MnO_3$ ($y = x/(2-x)$).

The differential thermal analysis (DTA) curves of $In_{0.8}MnO_{2.7}$ and $In_{0.7}MnO_{2.55}$ showed one broad exothermal peak staring at 953 K and centered at 973 K for $In_{0.8}MnO_{2.7}$ and starting at 873 K and centered at 933 K for $In_{0.7}MnO_{2.55}$. The XRD patterns collected after the DTA experiments showed that the samples had a cubic bixbyite-type structure with a lattice parameter of $a = 9.7597(1)$ Å for $(In_{0.889}Mn_{1.111})O_3$ and $a = 9.73447(5)$ Å for $(In_{0.824}Mn_{1.176})O_3$. The crystal structure of $(In_{0.824}Mn_{1.176})O_3$ has been investigated using synchrotron XRD.[14]

The dielectric constant of $In_{0.8}MnO_{2.7}$ demonstrated a strong frequency variation and a strong increase above about 200 K.[14] The tangent losses showed several relaxation processes (several broad frequency-dependent anomalies). This behavior is often observed in perovskite-type oxides and is attributed to the increased conductivity at high temperatures. Below about 100 K, the intrinsic dielectric constant could be measured, and the value is about 25–26. This value is close to the dielectric constant of $LnMnO_3$ (Ln = Tb–Lu) perovskites ($\varepsilon \approx 30$).[5] No anomalies were found on the dielectric constant of $In_{0.8}MnO_{2.7}$ at low temperatures except for a very weak downturn below 14 K. Dielectric properties of other $In_{1-x}MnO_{3-1.5x}$ samples with $x = 0.3$–0.5 could not be measured because the pellets were too loose to prepare good contacts.

$(In_{1-y}Mn_y)MnO_3$ ($1/9 \le y \le 1/3$) has the monoclinically distorted $GdFeO_3$-type perovskite structure (space group $P2_1/n$). $InCrO_3$ and $InRhO_3$ perovskites have the orthorhombic $GdFeO_3$-type perovskite structure (space group $Pnma$).[10] The $P2_1/n$ structure is observed in some B-site-ordered perovskites (for example, Sr_2YRuO_6 and La_2NiMnO_6)[16–18] because the $P2_1/n$ structure has two crystallographically independent B sites and one A site. What is the origin of the monoclinic distortion in $(In_{1-y}Mn_y)MnO_3$?

The BVS values show that the Mn atoms at the Mn3 site are highly underbonded assuming the oxidation state +3. The BVS value of Mn3 is about +2.[14] If we assume that Mn atoms at the Mn3 site have the oxidation state +2, the charge compensation may be reached 1) by the formation of oxygen deficiencies, $(In_{1.5}^{3+}Mn_{0.5}^{2+})_A(Mn^{3+})_{B1}(Mn^{3+})_{B2}O_{5.75}$ ($Z = 2$) and 2) by formation of Mn^{4+}, $(In_3^{3+}Mn^{2+})_A(Mn^{4+}Mn^{3+})_{B1}(Mn_2^{3+})_{B2}O_{12}$ ($Z = 1$), where A, B1, and B2 stand for the A site and two B sites of the perovskite structure. The structural analysis showed that all the oxygen sites are fully occupied. Furthermore, no change in the weight of platinum capsules was found during the high-pressure synthesis, thus confirming that the overall chemical composition should be kept. Therefore, we can rule out the first possibility.

The Mn2 site has a very strong Jahn–Teller distortion ($\Delta(Mn2) = 85.1 \times 10^{-4}$). This distortion is even larger than that of $LuMnO_3$ ($\Delta(Mn) = 75.3 \times 10^{-4}$).[3] This fact is in agreement with the general tendency that the Jahn–Teller distortion increases with decreasing Ln^{3+} radius.[3] Therefore, the Mn2 site should be occupied exclusively by Mn^{3+} ions (the BVS value is +3.21). On the other hand, the distortion of the Mn1 site in $(In_{0.75}Mn_{0.25})MnO_3$ is much smaller ($\Delta(Mn1) = 10.6 \times 10^{-4}$), and the BVS value of Mn1 is +3.27. (The absence of a strong Jahn–Teller distortion of the Mn1 site also gives support for ruling out the first possibility assumed above, because it cannot explain why the B1 and B2 sites with Mn^{3+} are different.) Therefore, the Mn1 site may have a statistical distribution of Mn^{3+} and Mn^{4+} ions. The structural data are consistent with the ion distribution as $(In_3^{3+}Mn^{2+})_A(Mn^{4+}Mn^{3+})_{B1}(Mn_2^{3+})_{B2}O_{12}$, and it explains why $(In_{1-y}Mn_y)MnO_3$ has the structure of the B-site-ordered perovskites. Note that in $Sr_{0.98}Mn_{0.02}TiO_3$, it was found that Mn atoms are located in both the A site (as Mn^{2+}) and the B site (as Mn^{4+}).[19] Therefore, the example of $Sr_{0.98}Mn_{0.02}TiO_3$ gives support for the proposed ion distribution in $(In_{0.75}Mn_{0.25})MnO_3$. The concentration of Mn^{2+} ions at the A site is much higher in $(In_{0.75}Mn_{0.25})MnO_3$ than in $Sr_{0.98}Mn_{0.02}TiO_3$. In light of the present results, it is interesting to investigate the distribution of transition metals[13] in

$(In_{1-y}M_y)MO_3$ ($y = 0.176$, $M = Mn_{0.5}Fe_{0.5}$), which has the polar *R*3*c* structure and long-range magnetic ordering near room temperature, because Mn atoms may be preferentially localized at the A site.[11] The *R*3*c* structure has one crystallographic B site, very similar M–O bond lengths, and, therefore, no Jahn–Teller distortion and no B-site ordering. In general, isovalent doping in the B site of $LnMnO_3$ (Ln = La–Lu) suppresses the Jahn–Teller distortion (especially at high doping levels). This scenario is probably realized during doping of $(In_{1-y}Mn_y)MnO_3$. Introduction of Fe^{3+} ions into $(In_{1-y}Mn_y)MnO_3$ suppresses the Jahn–Teller distortion and the tendency for Mn disproportionation and stabilizes the simpler *R*3*c* structure.

The proposed ion distribution can also explain in part peculiar magnetic properties of $(In_{1-y}Mn_y)MnO_3$. In the case of an undisturbed B sublattice with only Mn^{3+} ions, we would expect a long-range magnetic ordering near 40 K similar to other members of $LnMnO_3$ (Ln = Y, Ho–Lu).[3] For example, a clear antiferromagnetic peak was observed in $LuMnO_3$ near 40 K for magnetic susceptibilities without noticeable difference between the ZFC and FC curves.[20] However, spin-glass-like magnetic properties were found in $Lu_{1-y}Ca_yMnO_3$ ($0.1 \le y \le 0.5$)[20] and $Y_{0.7}Ca_{0.3}MnO_3$,[21] for which the B sublattice has random distribution of Mn^{3+} and Mn^{4+} ions. Note that not only the random distribution of Mn^{3+} and Mn^{4+} ions is responsible for spin-glass properties but also the competition between nearest-neighbor and next-nearest-neighbor interactions in $LuMnO_3$ and $YMnO_3$, because members with large Ln^{3+} ions show long-range magnetic ordering at high temperatures in solid solutions $La_{1-y}Ca_yMnO_3$ and $La_{1-x}Sr_xMnO_3$.[2]

Nevertheless, there are some differences between $(In_{1-y}Mn_y)MnO_3$ and $Ln_{1-y}Ca_yMnO_3$ (Ln = Y and Lu). $(In_{1-y}Mn_y)MnO_3$ has almost the same effective magnetic moment per mole of manganese ions (because Mn^{2+} and Mn^{4+} ions almost compensate each other in the calculation of the effective magnetic moment) and the same negative Curie–Weiss temperature independent of *y* (Figure 3). The deviation from linear Curie–Weiss behavior starts at higher temperatures for larger *y*, thus indicating that ferromagnetic-like interactions are enhanced with increasing manganese content. The transition temperatures increase with increasing *y* in $(In_{1-y}Mn_y)MnO_3$ ($1/9 \le y \le 1/3$). On the other hand, the transition temperatures decrease with increasing *y* in $(Lu_{1-y}Ca_y)MnO_3$ ($0 \le y \le 0.3$).[20] The Curie–Weiss temperature changes its sign from negative to positive in $Ln_{1-y}Ca_yMnO_3$ (Ln = Y and Lu) near $y = 0.3$. Magnetic properties typical for canted antiferromagnets were observed in $(Lu_{1-y}Ca_y)MnO_3$ only for $0.9 \le y \le 1$,[20] while those in $(In_{1-y}Mn_y)MnO_3$ were observed for $y = 1/3$. The different magnetic behavior of $(In_{1-y}Mn_y)MnO_3$ is probably the effect of the B-site ordering of Mn^{3+} and Mn^{4+} ions and the presence of Mn^{2+} ions at the A site. Mn^{2+} ions ($S = 5/2$) at the A sites (especially when their concentration is high) may interact with Mn ions at the B sites and strongly influence the magnetic properties. However, we note that magnetic rare-earth ions at the A sites usually have little influence on the magnetic properties of the B sublattice, and long-range magnetic ordering is observed in B-site-ordered perovskites even when one B atom is nonmagnetic, for example, Sr_2YRuO_6.[16]

No ferroelectric transitions were detected in $(In_{1-y}Mn_y)MnO_3$ ($y = 0.111$) at low temperatures, in contrast to $LnMnO_3$ (Ln = Tb–Lu) perovskites.[5] This result also shows that $(In_{1-y}Mn_y)MnO_3$ and $LnMnO_3$ are different.

On heating, $(In_{1-y}Mn_y)MnO_3$ transforms into the cubic bixbyite-type $(In_{2-z}Mn_z)O_3$ solid solution ($1.111 \le z \le 1.176$). At ambient pressure, the solubility of transition metals in In_2O_3 is rather small ($z \approx 0.1$ for M = Mn,[22] $z \approx 0.15$ for M = Cr,[23] and $z \approx 0.5$ for M = Fe).[24] Magnetic properties of $(In_{2-z}M_z)O_3$ have attracted tremendous interest as diluted magnetic semiconductor systems.[25] The origin of room-temperature ferromagnetic-like properties in $(In_{2-z}M_z)O_3$ has been discussed a lot. It appears that the ferromagnetism is not due to the spins of the transition metal ions but to defects created under certain experimental conditions.[25] Perovskites $(In_{1-y}Mn_y)MnO_3$ can give bixbyite-type $(In_{2-z}Mn_z)O_3$ with a record high concentration of Mn ions. For example, $(In_{1-y}Mn_y)MnO_3$ with $y = 0.176$ gives $(In_{0.824}Mn_{1.176})O_3$ with the cubic lattice parameter $a = 9.73447(5)$ Å (cf. $a = 10.1188$ Å for In_2O_3 and $a = 9.9462$ Å for $(In_{1.5}Fe_{0.5})O_3$).[24] We have investigated the magnetic properties of $(In_{0.824}Mn_{1.176})O_3$. We found only the Curie–Weiss behavior with $\mu_{eff} = 4.97\,\mu_B$ per Mn^{3+} (the calculated value is $4.90\,\mu_B$) and $\theta = -54$ K with a very weak ferromagnetic-like anomaly near 43 K arising from the presence of a trace amount of the ferrimagnetic impurity Mn_3O_4.[14] Therefore, only paramagnetic properties were observed in the bixbyite-type $(In_{2-z}Mn_z)O_3$ solid solution even with a very high concentration of Mn atoms.

In conclusion, we have prepared new perovskite oxides $(In_{1-y}Mn_y)MnO_3$ ($1/9 \le y \le 1/3$) using a high-pressure high-temperature technique. It is proposed that the doping at the A site of a perovskite occurs with Mn^{2+} ions, and $(In_{1-y}Mn_y)MnO_3$ compounds are similar with $(Lu_{1-y}Ca_y)MnO_3$ and other related doped manganites. Ordering of Mn^{3+} and Mn^{4+} ions is proposed to explain the B-site-ordered structure of $(In_{1-y}Mn_y)MnO_3$. $(In_{1-y}Mn_y)MnO_3$ ($1/9 \le y \le 0.25$) demonstrates spin-glass-like properties, and only $(In_{2/3}Mn_{1/3})MnO_3$ shows magnetic properties typical for canted antiferromagnets with $T_N = 70$ K. During heating in air, $(In_{1-y}Mn_y)MnO_3$ perovskites transform to cubic $(In_{2-z}Mn_z)O_3$ ($1.111 \le z \le 1.176$) with record high concentrations of Mn ions.

Experimental Section

$In_{1-x}MnO_{3-1.5x}$ samples with $x = 0.1$, 0.2, 0.3, 0.4, and 0.5 were prepared from stoichiometric mixtures of In_2O_3 (99.99%, Rare Metallic Co. Ltd.) and Mn_2O_3. Single-phase Mn_2O_3 was prepared by heating MnO_2 (99.99%, Rare Metallic Co. Ltd.) in air at 923 K for 24 h. The synthesis was performed in a belt-type high-pressure apparatus at 6 GPa and 1773 K for 40 min in Pt capsules. After heat treatment, the samples were quenched to room temperature, and the pressure was slowly released. The resultant samples were black dense ($x = 0.1$ and 0.2) and loose ($x = 0.3$–0.5) pellets.

X-ray powder diffraction (XRD) data were collected at room temperature on a RIGAKU Ultima III diffractometer using $Cu_{K\alpha}$ radiation ($2\theta = 10$–$150°$, step width 0.02°, counting time 10 s per step). Synchrotron XRD data were measured at room temperature on a large Debye–Scherrer camera at the BL15XU beam line of SPring-

8.[26] The data were collected between 5° and 60° with a 0.003° interval in 2θ. The incident beam was monochromated at $\lambda = 0.65297$ Å. The sample packed into a Lindenmann glass capillary (inner diameter: 0.1 mm) was rotated during the measurement. The Rietveld analysis was performed with RIETAN-2000.[27]

Magnetic susceptibilities $\chi = M/H$ were measured on a SQUID magnetometer (Quantum Design, MPMS) between 2 and 400 K in applied fields of 100 Oe, 1 kOe, and 10 kOe under both zero-field-cooled (ZFC) and field-cooled (FC; on cooling) conditions. Isothermal magnetization measurements were performed between −50 and 50 kOe at 5 K. Specific heat C_p at magnetic fields of 0 and 70 kOe was recorded between 2 and 300 K on cooling and heating by a pulse relaxation method using a commercial calorimeter (Quantum Design PPMS). A large hysteresis was found for the specific heat of $LnMnO_3$ (Ln = Ho–Lu) during heating and cooling because of the first-order phase transition.[3] In $In_{1-x}MnO_{3-1.5x}$, no differences were observed on heating and cooling on the specific heat curves. The differential thermal analysis (DTA) was performed in air on a MAC Science TG-DTA 2000 instrument at a heating/cooling rate of 10 K min^{-1} up to 1000 K. Dielectric constant was measured using an Agilent E4980 A LCR meter between 5 and 300 K in the frequency range of 100 Hz and 1 MHz.

Received: May 21, 2010
Revised: July 1, 2010
Published online: September 6, 2010

Keywords: dielectric properties · indium · magnetic properties · manganese · perovskites

[1] R. H. Mitchell, *Perovskites: Modern and Ancient*; Almaz, Thunder Bay, Ontario, **2002**.
[2] D. M. Edwards, *Adv. Phys.* **2002**, *51*, 1259.
[3] M. Tachibana, T. Shimoyama, H. Kawaji, T. Atake, E. Takayama-Muromachi, *Phys. Rev. B* **2007**, *75*, 144425.
[4] T. Kimura, T. Goto, H. Shintani, K. Ishizaka, T. Arima, Y. Tokura, *Nature* **2003**, *426*, 55.
[5] V. Yu. Pomjakushin, M. Kenzelmann, A. Doenni, A. B. Harris, T. Nakajima, S. Mitsuda, M. Tachibana, L. Keller, J. Mesot, H. Kitazawa, E. Takayama-Muromachi, *New J. Phys.* **2009**, *11*, 043019.
[6] D. G. Tomuta, S. Ramakrishnan, G. J. Nieuwenhuys, J. A. Mydosh, *J. Phys. Condens. Matter* **2001**, *13*, 4543.
[7] a) J. E. Greedan, M. Bieringer, J. F. Britten, D. M. Giaquinta, H. C. zur Loye, *J. Solid State Chem.* **1995**, *116*, 118; b) A. A. Belik, S. Kamba, M. Savinov, D. Nuzhnyy, M. Tachibana, E. Takayama-Muromachi, V. Goian, *Phys. Rev. B* **2009**, *79*, 054411.
[8] K. Uusi-Esko, J. Malm, N. Imamura, H. Yamauchi, M. Karppinen, *Mater. Chem. Phys.* **2008**, *112*, 1029.
[9] J. H. Park, J. B. Parise, *Mater. Res. Bull.* **1997**, *32*, 1617.
[10] R. D. Shannon, *Inorg. Chem.* **1967**, *6*, 1474.
[11] A. A. Belik, T. Furubayashi, Y. Matsushita, M. Tanaka, S. Hishita, E. Takayama-Muromachi, *Angew. Chem.* **2009**, *121*, 6233; *Angew. Chem. Int. Ed.* **2009**, *48*, 6117.
[12] E. Kan, H. Xiang, C. Lee, F. Wu, J. Yang, M.-H. Whangbo, *Angew. Chem.* **2010**, *122*, 1647; *Angew. Chem. Int. Ed.* **2010**, *49*, 1603.
[13] J. A. Alonso, *ChemPhysChem* **2010**, *11*, 58.
[14] See the Supporting Information.
[15] R. E. Brese, M. O'Keeffe, *Acta Crystallogr. Sect. B* **1991**, *47*, 192.
[16] P. D. Battle, W. J. Macklin, *J. Solid State Chem.* **1984**, *52*, 138.
[17] C. L. Bull, D. Gleeson, K. S. Knight, *J. Phys. Condens. Matter* **2003**, *15*, 4927.
[18] N. S. Rogado, J. Li, A. W. Sleight, M. A. Subramanian, *Adv. Mater.* **2005**, *17*, 2225.
[19] I. Levin, V. Krayzman, J. C. Woicik, A. Tkach, P. M. Vilarinho, *Appl. Phys. Lett.* **2010**, *96*, 052904.
[20] N. Imamura, M. Karppinen, T. Motohashi, H. Yamauchi, *Phys. Rev. B* **2008**, *77*, 024422.
[21] R. Mathieu, P. Nordblad, D. N. H. Nam, N. X. Phuc, N. V. Khiem, *Phys. Rev. B* **2001**, *63*, 174405.
[22] D. Bérardan, E. Guilmeau, D. Pelloquin, *J. Magn. Magn. Mater.* **2008**, *320*, 983.
[23] L. Bizo, M. Allix, H. Niu, M. J. Rosseinsky, *Adv. Funct. Mater.* **2008**, *18*, 777.
[24] D. Bérardan, E. Guilmeau, *J. Phys. Condens. Matter* **2007**, *19*, 236224.
[25] J. M. D. Coey, *Curr. Opin. Solid State Mater. Sci.* **2006**, *10*, 83.
[26] M. Tanaka, Y. Katsuya, A. Yamamoto, *Rev. Sci. Instrum.* **2008**, *79*, 075106.
[27] F. Izumi, T. Ikeda, *Mater. Sci. Forum* **2000**, *321–324*, 198.

